Damage Assessment of Hydrokinetic Composite Turbine Blades

Steve E. Watkins[1*], *Senior Member SPIE*, Kevin E. Robison[1], James R. Nicholas[2],
Greg A. Taylor[2], K. Chandrashekhara[2], and Joshua L. Rovey[2]
[1]Department of Electrical and Computer Engineering and
[2]Department of Mechanical and Aerospace Engineering
Missouri University of Science & Technology, Rolla, Missouri 65409, USA

ABSTRACT

Damage assessment of composite blades is investigated for hydrokinetic turbine applications in which low-velocity impact damage is possible. The blades are carbon/epoxy laminates that are made using an out-of-autoclave process and the blade design is a hydrofoil with constant cross-section. Both undamaged and damaged blades are manufactured and instrumented with strain sensors. Water tunnel testing is conducted with varying flow velocities and for different blade angles. A theoretical simulation is included that is based on finite-element method. The influence of damage on the response characteristics is discussed as an indicator of structural health.

Index Terms – health monitoring, composite blades, strain analysis, smart structures

1. INTRODUCTION

Hydrokinetic systems utilize the kinetic energy of flowing water to generate power [1]. Such systems are potential sources of renewable energy from both rivers and ocean tides [2-3]. Economic studies have encouraged the development of hydrokinetic technology [4]. Important aspects of any field implementation are operating and life cycle costs associated with inspection and maintenance. While the electrical behavior of hydrokinetic systems can be monitored, structural health monitoring technology for system components has not been well developed. In particular, rotating blades and turbines are typical elements in hydrokinetic systems and they are subject to extreme marine conditions.

Smart structures technology is an interdisciplinary approach to health monitoring [5]. It requires knowledge of materials and sensors as well as the application. Composite materials and strain sensing are the topics relevant to this work. Composite materials have been applied in many areas including those for marine environments. Its use in turbine blades is an ongoing area of study. Strain sensors of many types have been used to characterize composite materials. The use of sensors in moving structures creates new challenges as opposed to monitoring behavior in static load bearing applications. Our prior work has examined the behavior and characterization of composites using strain sensing [6-10]. We have made preliminary investigations of composite turbine blades [11]. This work extends prior experiments by investigating more practical blade designs and blade performance in water.

In this work, composite blade performance and instrumentation are investigated. Three-dimensional, multilayer blades are considered for static loading and water flow testing. These structures are carbon/epoxy, symmetric composite laminates that were manufactured using an autoclave process. Performance of both undamaged and damaged blades is investigated to determine load-induced strain as an indicator of structural health. Experimental results for strain measurements from electrical resistance gages are presented in preparation for later embedded sensors. Also, theoretical strain characteristics are presented from in-house, finite element analysis for all sample cases.

* Author E-mail Addresses: steve.e.watkins@ieee.org, chandra@mst.edu, and roveyj@mst.edu
Contact Author: S. Watkins. 121 EECH, Missouri University of Science and Technology (formerly University of Missouri-Rolla), 301 W. 16th St., Rolla 65409-0040 573-341-6321, Fax 573-341-4532

Nondestructive Characterization for Composite Materials, Aerospace Engineering, Civil Infrastructure, and Homeland Security 2013, edited by Tzu Yang Yu, Andrew L. Gyekenyesi, Peter J. Shull, Aaron A. Diaz, H. Felix Wu, Proc. of SPIE Vol. 8694, 86942B · © 2013 SPIE · CCC code: 0277-786X/13/$18 · doi: 10.1117/12.2009840

2. STRUCTURES

2.1 Hydrokinetic Turbine Health Monitoring

Hydrokinetic turbine systems generate energy from flowing water current. The blades are underwater in either horizontal-axis or vertical-axis designs. Hence, the blades are subject to extreme marine conditions and to impacts from ice, debris, etc. The turbine location depends on the presence of strong currents or tides. Also, potential locations are constrained by activities such as shipping or fishing, seasonal current variations, and environmental concerns. Hence, appropriate locations are typically remote. Consequently, monitoring, inspection, and maintenance will be difficult and costly. System economics will be greatly influenced by these operating costs. The structural health of blades as a critical element must be assured so that minor damage or fatigue does not progress to catastrophic failure. Physical blade inspections would need to be conservatively scheduled and would involve system downtime and perhaps partial disassembly. A better alternative might be in-situ monitoring. Note an important difficulty with in-situ monitoring is relaying sensor data from the rotating blade to the outside world. A physical connection via an electrical wire or an optical fiber is not practical in the rotating machine.

Composite turbine blades are the focus of this work. Composite materials are well suited for marine environments with regard to ruggedness, weight, structural flexibility, and corrosion resistance. A health monitoring approach for composite turbines blades was proposed and preliminary experiments described in prior work [11,12]. This smart structures system uses in-situ strain sensors, embedded support electronics, and acoustic data transmission as shown in Figure 1(a). Composite materials are known to be compatible with embedded sensors [9]. Good candidates for permanent strain instrumentation are fiber optic sensors based on Fabry-Perot interferometric or Bragg designs [9,13-15]. (Electrical resistance gages are used in this study of composite blade performance due to reduced instrumentation cost and the laboratory environment.) Support electronics for the sensor demodulation and data transmission must be embedded in the rotating structure, e.g. the blade hub. Advances in sensor demodulation techniques and sensor motes and nodes have demonstrated the feasibility of miniaturized electronic packages [16-20]. The data are transmitted with an acoustic transducer to a receiver in a nearby base station.

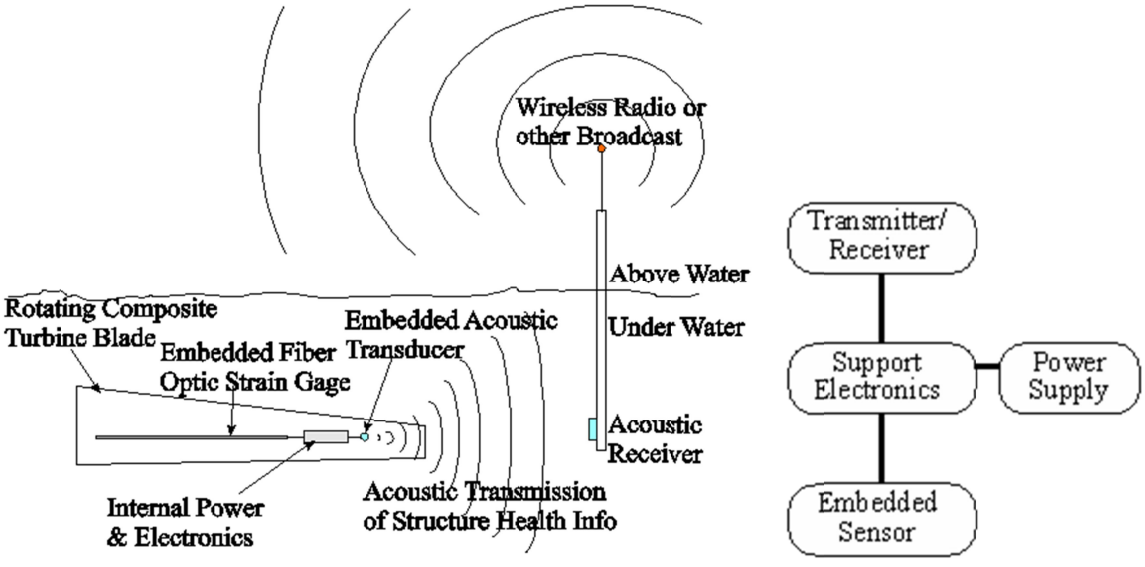

Figure 1. (a) Proposed Smart Health Monitoring System and (b) Major Subsystems.

Major sub-systems are shown in Figure 1(b). Functions of strain sensing, sensor demodulation, sensor data pre-processing, and data transmission must be embedded in the blade and hub assembly. The damage-induced strain characteristics for the composite blades must be understood to tailor the sensor sub-system, the sensor date pre-processing, and the data interpretation. Data interpretation must be must be done either in the support electronics, in the receiver base station, or in a combination. Also, the data capacity of the acoustic data transmission will depend on the degree of pre-processing available in the embedded electronics. The ultimate objective of the health monitoring system is to provide a warning if blade structure is compromised. The health information may be detailed, in which case the degree of damage and location is detected, or may be a simple warning that the blade needs attention and that the system operation must be adjusted.

2.2 Sample Composite Beams and Blades

Two three-dimensional composite blades were manufactured for testing using an out-of-autoclave process in the Composites Fabrication Laboratory at Missouri University of Science and Technology. A hydrofoil blade design was used. One blade was undamaged; the other blade was identical except for prescribed damage. This second blade was compromised structurally by a hole of 2.54 cm (1.0 in.) diameter that is centered 15.24 cm (6.0 in.) from the blade root. The hole is in both the top and bottom surface of the blade.

Both the damaged and undamaged blades are shown in Figure 2. The blade geometry has a constant cross section based on Eppler E395 airfoil, with a chord length of 5.08 cm (2.00 in.) and a span of 25.4 cm (10.0 in.). There is a 2.54 cm (1.0 in.) transition from the airfoil to a 0.8 cm (0.32 in.) diameter root section. The root section is 2.54 cm (1.0 in.) in length. Strain instrumentation for the blades was applied after fabrication and consisted of three surface-mounted electrical strain gages. The gages were located on the convex surface, 2.54 cm (1.0 in.) from the leading edge. The locations along the blade length were at 10.16 cm (4.0 in.), 14.92 cm (5.88 in.), and 20.32 cm (8.00 in.) from the root.

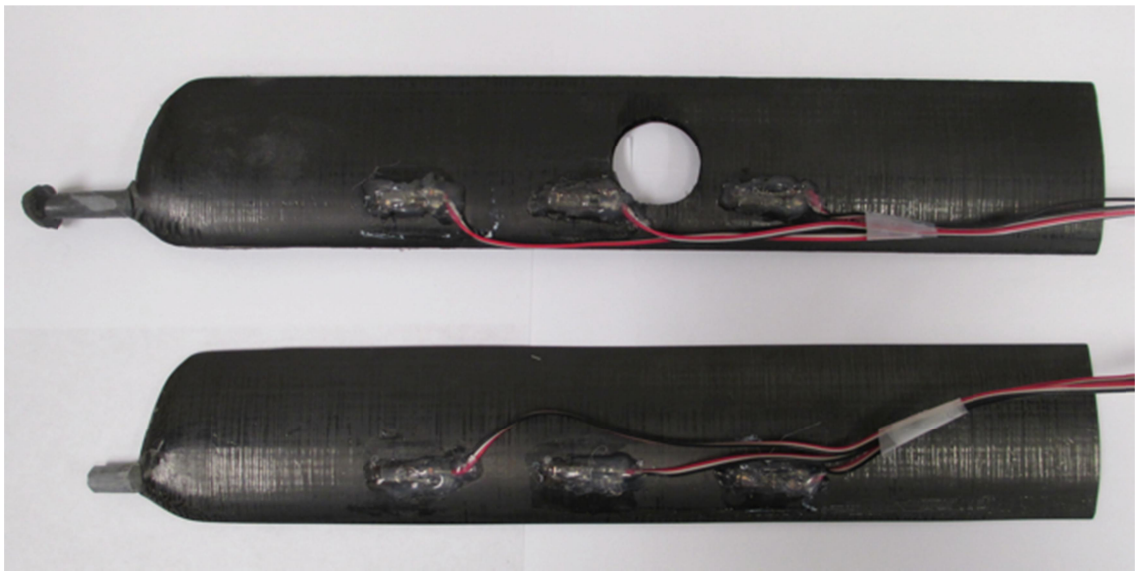

Figure 2. Damaged (top) and Undamaged (bottom) Composite Blades.

A cross sectional view of the hydrofoil manufactured is shown in Figure 3. The hydrofoil is composed of an upper and a lower half. Both halves were manufactured by a single out-of–autoclave process using Cycom 5250, a unidirectional carbon fiber prepreg. The fiber was layed-up on the mold in a three layer configuration of [90°/0°/90°], with 0° along the hydrofoil span. The two halves were vacuumed sealed to the mold and cured using the cycle provided by Cytec, the prepreg manufacturer. Once cured, excess material was removed and the halves were then bonded together using a two-part phenolic epoxy. The root section was then formed from particulate reinforced epoxy putty using a two-part mold and cured at room temperature.

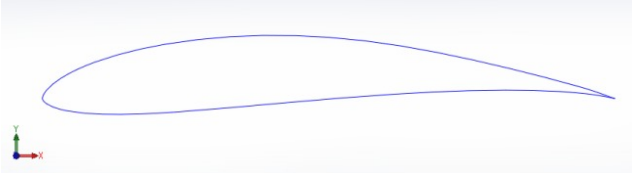

Figure 3. Cross Sectional View of Hydrofoil.

Basic information related to the three-layer composite blade, in terms of material type and lay-up is listed in Table 1. Material properties of the composite blades are listed in Table 2.

Table 1. Basic Information for the Three-layer Composite Blade.

Material Type	CYTEC (Cycom 5320/AS4)
Lamina Thickness	0.127 cm (0.005 in.)
Lay-up Sequence	[90/0/90]

Table 2. Material Properties for the Three-layer Composite Blade.

Young's Modulus	E_{11} = 143 GPa
	$E_{22} = E_{33}$ = 10.19 GPa
Poisson's Ratio	$\nu_{12} = \nu_{13} = \nu_{23}$ = 0.3
Shear Modulus	$G_{12} = G_{13}$ = 4.01 GPa
	G_{23} = 3.70 GPa
Density	ρ = 1580 kg/m^3

2.3 Finite Element Analysis of Composite Structures

A theoretical analysis was performed using the blade element momentum finite element method (BEM-FEM) under cantilever boundary conditions. Loading conditions were matched to the experimental tests that are described in later sections. Flexure strains at each sensor location were obtained for a static (in air) case with a mass placed at 24.13 cm (9.5 in.) from the root. Flexure strains at each sensor location were obtained for a water flow case with specific conditions for water velocity and blade pitch angle. For the later case, hydrofoil theory was used to integrate the force over the boundary of the hydrofoil and obtain the normal and tangential (reference to the blade chord surface) loadings. The normal/tangential loadings were then applied on the blade surface using finite element method.

Load calculation:

At specified angle of attack α, the lift and drag coefficients C_l and C_d are extrapolated from the hydrofoil table which includes the relationship between C_l / $C_d$and α. The lift L and drag D per unit length can be computed by

$$L = \frac{1}{2}\rho U^2 c C_l$$

$$D = \frac{1}{2}\rho U^2 c C_d$$

where ρ is flow density, U is flow velocity and c is chord length. The force normal to and tangential to the blade can be obtained by

$$F_N = L\cos\alpha + D\sin\alpha$$

$$F_T = L\sin\alpha - D\cos\alpha$$

These loads serve as the input to the finite element model.

Figure 4 and Figure 5 show the finite element model for the undamaged and damaged composite blades, respectively. Hydrodynamic loadings are applied as concentrated forces on the blade surface at different stations using MPC (Multi-point constraint) technique. The sensor locations are indicated.

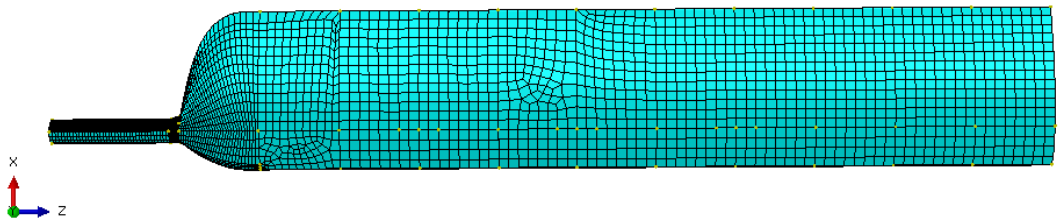

Figure 4. Finite Element Model of the Composite Blade.

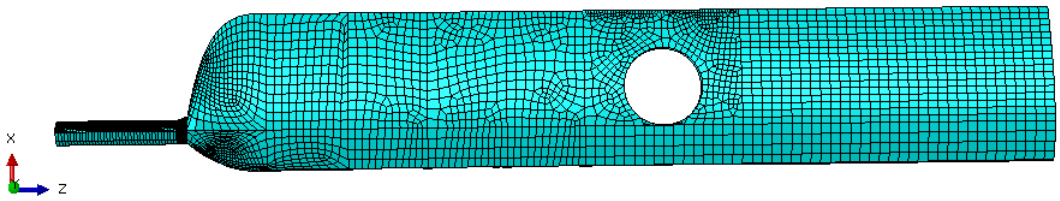

Figure 5. Finite Element Model of the Damaged Composite Blade.

3. EXPERIMENTAL PROCEDURE

3.1 Strain Instrumentation

The three electrical resistance strain gages were located for flexure measurement as shown in Figure 6 and Figure 7. These gages were 120-Ω electrical resistance gages (Micro-Measurements EA series) and the gage lengths were 6.35 mm (0.25 in.). The gages were surface mounted with M-Bond 200 adhesive. The support instrumentation was a Wheatstone bridge strain indicator (Micro-Measurements P-3500) and an oscilloscope. The strain readings were averaged for about one minute each and varied about ±1 microstrain.

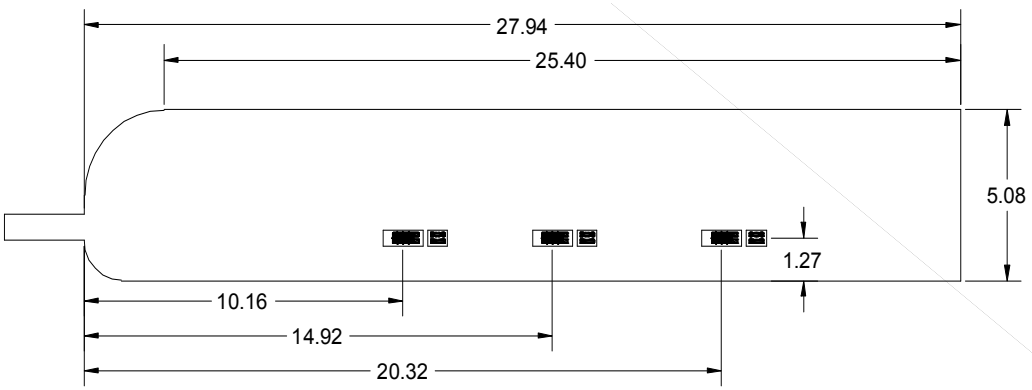

Figure 6. Undamaged Carbon/Epoxy Composite Blade with Sensor Layout (all units in cm).
The sensor locations are 1, 2, and 3 from left to right.

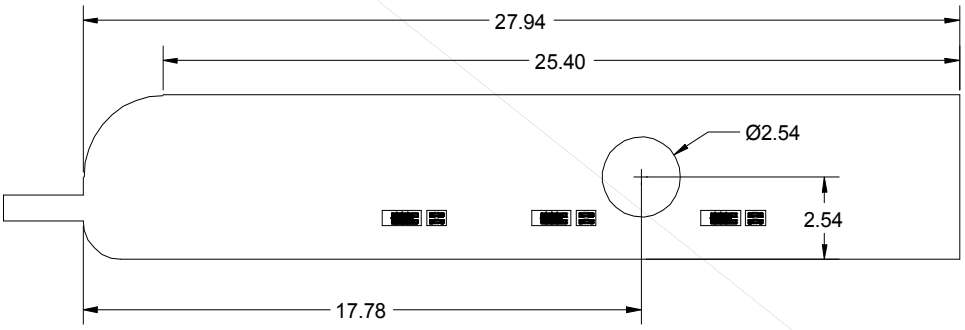

Figure 7. Damaged Carbon/Epoxy Composite Blade with Sensor Layout (all units in cm).
The sensor locations are 1, 2, and 3 from left to right.

3.2 Strain Measurements

The static test case was to determine the static flexural strain. The undamaged blade was clamped horizontally in the mounting hub and a mass of 244.3 grams was placed 24.13 cm from the root of the blade, as shown in Figure 8. The average strain values were then recorded. This test was then repeated for the damaged blade.

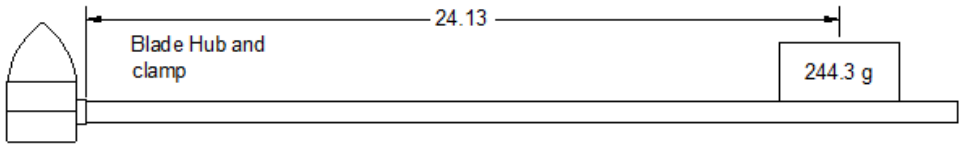

Figure 8. Experimental Setup of Static Blade Test.

The water flow test was done for both undamaged and damaged blades in the Water Tunnel Laboratory at Missouri S&T. The facility is a Rolling Hills Research Corp. model 1520-HK water tunnel capable of laminar flow up to 1 m/s (1.9 kts) and has a testing cross section of 38.1x50.8 cm and length of 152.4 cm. The experimental setup is shown in Figure 9. The blades were attached to a mounting hub and positioned vertically in the water with the sensors on downstream side. The entire blade and hub were submerged. Details of the blade arrangement are shown in Figure 10.

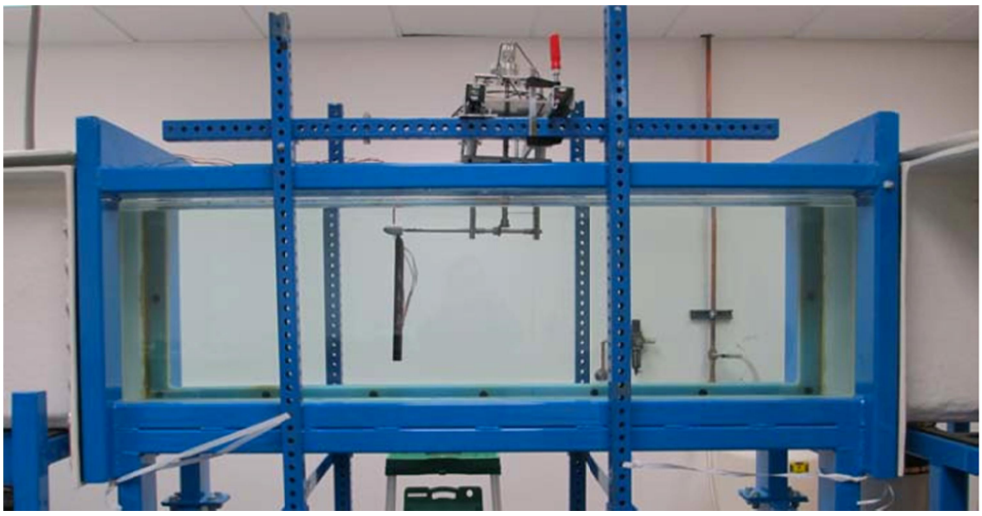

Figure 9. Experimental Setup of Water Flow Test.

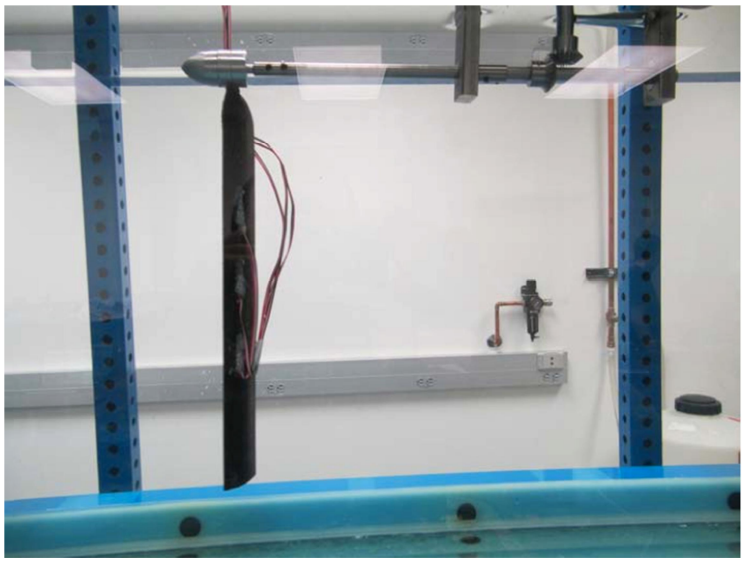

Figure 10. Detail of a Blade in the Water Tunnel.

The hub allowed the blades to be positioned at various pitch angles (or angles of attack). For a 0° angle of attack, the blade was aligned with the water flow. For a 90° angle of attack, the blade was perpendicular to the flow. Strain measurements were recorded at all three gage locations for angles of attack of 50°, 60°, 70°, and 80° for water speeds of 0.11, 0.22, and 0.31 m/s.

4. RESULTS AND ANALYSIS

Results of the static blade loading are shown in Table 3. Strain 1, 2, and 3 are the strain values in microstrain from sensor locations 1, 2, and 3, respectively. Results are shown for the undamaged blade for all locations. The damaged blade root section broke after the data for location 1 was taken. The blades were stiff and the damage made little difference in the strain value at the first sensor location.

Table 3. Experimental Strain Values for Static Loading.

Blade type	Strain 1 (microstrain)	Strain 2 (microstrain)	Strain 3 (microstrain)
	Measured	Measured	Measured
Undamaged blade	-130 ±1	-91 ±1	-43 ±1
Damaged blade	-127 ±1	NA	NA

Results of the water flow loading at 0.11 m/s, 0.22 m.s, and 0.31 m/s are shown in Table 4, Table 5, Table 6, and Table 7. The tables record the strain values for blade angles of attack at 50°, 60°, 70°, and 80°, respectively. Both simulation values from the finite element analysis and the experimental (measured) values from the water tunnel are shown and a comparison of simulation and experimental values demonstrate good correlation. The strains are compressive as expected and the strain magnitudes are largest near the blade root. The strain magnitudes generally increase for higher flow velocities and larger angles of attack. The damage in the second blade had a subtle effect on strain and tended to change the strain at location 1 the most. The percent differences in the strain values at location 1 are shown in Table 8. The values at locations 2 and 3 were so small and measurement variations (±1 microstrain) so significant that quantitative comparisons are difficult. The differences are calculated as

Percent Difference = 100% x |Simulated Strain – Measured Strain|/|Simulated Strain|

Note that the closest matches tend to occur for the higher magnitudes of strain in which the signal-to-noise ratios of the measured results are better. Example trends at a 70° angle for flow velocities of 0.11 m/s and 0.31 m/s are plotted in Figure 11 and Figure 12, respectively.

Table 4. Strain Values in Water Tunnel (angle of attack: 50°).

		Strain 1 (microstrain)		Strain 2 (microstrain)		Strain 3 (microstrain)	
Blade type	Flow velocity	Simulated	Measured	Simulated	Measured	Simulated	Measured
Undamaged blade	0.11 m/s	-4.16	-2 ±1	-2.64	-3 ±1	-0.046	-2 ±1
	0.22 m/s	-16.5	-10 ±1	-10.5	-10 ±1	-1.82	-3 ±1
	0.31 m/s	-33.0	-34 ±1	-20.8	-18 ±1	-3.58	-6 ±1
Damaged blade	0.11 m/s	-4.37	-8 ±1	-2.28	-6 ±1	-2.75	-4 ±1
	0.22 m/s	-17.5	-20 ±1	-9.15	-14 ±1	-4.01	-5 ±1
	0.31 m/s	-34.7	-37 ±1	-18.2	-27 ±1	-5.03	-6 ±1

Table 5. Strain Values in Water Tunnel (angle of attack: 60°).

		Strain 1 (microstrain)		Strain 2 (microstrain)		Strain 3 (microstrain)	
Blade type	Flow velocity	Simulated	Measured	Simulated	Measured	Simulated	Measured
Undamaged blade	0.11 m/s	-4.37	-4 ±1	-2.75	-3 ±1	-0.500	-2 ±1
	0.22 m/s	-17.5	-12 ±1	-11.0	-10 ±1	-2.00	-10 ±1
	0.31 m/s	-34.7	-36 ±1	-21.6	-20 ±1	-3.94	-19 ±1
Damaged blade	0.11 m/s	-4.60	-3 ±1	-2.36	-6 ±1	-1.24	0 to 1
	0.22 m/s	-18.4	-13 ±1	-9.45	-11 ±1	-4.01	-2 ±1
	0.31 m/s	-36.6	-37 ±1	-18.8	-26 ±1	-5.02	-6 ±1

Table 6. Strain Values in Water Tunnel (angle of attack: 70°).

		Strain 1 (microstrain)		Strain 2 (microstrain)		Strain 3 (microstrain)	
Blade type	Flow velocity	Simulated	Measured	Simulated	Measured	Simulated	Measured
Undamaged blade	0.11 m/s	-4.58	-4 ±1	-2.87	-3 ±1	-0.545	-2 ±1
	0.22 m/s	-18.3	-13 ±1	-11.5	-10 ±1	-2.17	-4 ±1
	0.31 m/s	-36.3	-30 ±1	-22.6	-25 ±1	-4.27	-10 ±1
Damaged blade	0.11 m/s	-4.83	-7 ±1	-2.44	-3 ±1	-1.26	-3 ±1
	0.22 m/s	-19.3	-17 ±1	-9.75	-13 ±1	-3.99	-8 ±1
	0.31 m/s	-38.4	-40 ±1	-19.5	-26 ±1	-5.00	-10 ±1

Table 7. Strain Values in Water Tunnel (angle of attack: 80 °).

		Strain 1 (microstrain)		Strain 2 (microstrain)		Strain 3 (microstrain)	
Blade type	Flow velocity	Simulated	Measured	Simulated	Measured	Simulated	Measured
Undamaged blade	0.11 m/s	-4.73	-4 ±1	-2.96	-3 ±1	-0.575	-1 ±1
	0.22 m/s	-18.9	-16 ±1	-11.8	-11 ±1	-2.29	-5 ±1
	0.31 m/s	-37.5	-38 ±1	-22.1	-26 ±1	-4.51	-11 ±1
Damaged blade	0.11 m/s	-5.00	-4 ±1	-2.50	-3 ±1	-2.75	-3 ±1
	0.22 m/s	-20.0	-16 ±1	-10.0	-11 ±1	-3.98	-5 ±1
	0.31 m/s	-39.7	-42 ±1	-20.0	-26 ±1	-4.97	-11 ±1

Table 8. Percent Difference in Strain Values for Strain 1.

		Strain 1 (microstrain) angle of attack: 50 °			Strain 1 (microstrain) angle of attack: 60 °		
Blade type	Flow velocity	Simulated	Measured	Percent Difference	Simulated	Measured	Percent Difference
Undamaged blade	0.11 m/s	-4.16	-2 ±1	51.9%	-4.37	-4 ±1	8.5%
	0.22 m/s	-16.5	-10 ±1	39.4%	-17.5	-12 ±1	31.4%
	0.31 m/s	-33.0	-34 ±1	3.0%	-34.7	-36 ±1	3.7%
Damaged blade	0.11 m/s	-4.37	-8 ±1	83.1%	-4.60	-3 ±1	34.8%
	0.22 m/s	-17.5	-20 ±1	14.3%	-18.4	-13 ±1	29.3%
	0.31 m/s	-34.7	-37 ±1	6.6%	-36.6	-37 ±1	1.1%
		Strain 1 (microstrain) angle of attack: 70 °			Strain 1 (microstrain) angle of attack: 80 °		
Blade type	Flow velocity	Simulated	Measured	Percent Difference	Simulated	Measured	Percent Difference
Undamaged blade	0.11 m/s	-4.58	-4 ±1	12.7%	-4.73	-4 ±1	15.4%
	0.22 m/s	-18.3	-13 ±1	29.0%	-18.9	-16 ±1	15.3%
	0.31 m/s	-36.3	-30 ±1	17.4%	-37.5	-38 ±1	1.3%
Damaged blade	0.11 m/s	-4.83	-7 ±1	44.9%	-5.00	-4 ±1	20.0%
	0.22 m/s	-19.3	-17 ±1	11.9%	-20.0	-16 ±1	20.0%
	0.31 m/s	-38.4	-40 ±1	4.2%	-39.7	-42 ±1	5.8%

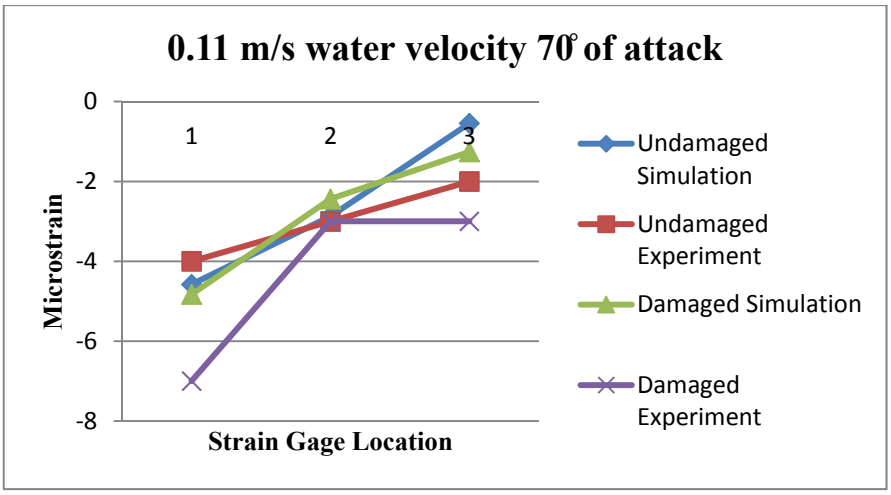

Figure 11. Trend Chart for Strain at 70° Angle of Attack and 0.11 m/s Flow Velocity.

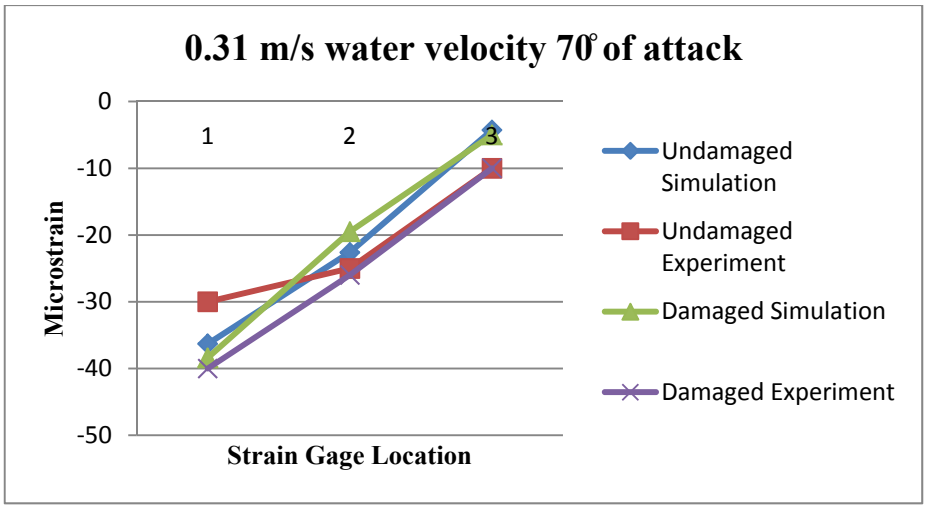

Figure 12. Trend Chart for Strain at 70° Angle of Attack and 0.31 m/s Flow Velocity.

5. SUMMARY AND HEALTH MONITORING DISCUSSION

Strain characteristics of composite blades were investigated for water turbine applications. Three-dimensional blades were successfully fabricated and strain instrumentation was attached. One blade was undamaged and the other was structurally compromised. Finite element simulation results generally matched experimental strain behavior. For the higher magnitudes of measured strain, in which the signal-to-noise ratio was better, the simulation and the experimental results matched the best. For instance, the simulation and measured values in the case of sensor location 1 and 0.31 m/s flow velocity had percent differences of less than 7%. The work demonstrates a capability to manufacture composite blades and to test the blades in a water tunnel environment.

The strain behavior in the water tunnel shows a strong dependence on water flow and blade angle of attack. The presence of damage tended to increase the strain magnitude especially near the blade root. However, the change in strain due to blade damage was very small even though the blade damage was significant. As a health monitoring parameter, a more detailed knowledge of strain in the blade, e.g. through a sensor array, may be needed as an indictor of damage. Also, strain monitoring may need to be combined with other parameters or information, such as power or vibration changes, to predict damage. Future work should look at a more complete understanding of strain in blades, especially as a function of the severity and location of damage. Expected strain levels in field implementations should be determined. Sensor number and placement may be important considerations for an effective monitoring system.

ACKNOWLEDGEMENTS

The authors wish to thank the Office of Naval Research (grant N00014-10-0923), the Department of Energy (grant DE-EE0004569), and the Office of Naval Research (contract ONR N000141010923 with Program Manager- Dr. Michele Anderson) for supporting this work.

REFERENCES

[1] Khan, M. J., Bhuyan, G., Iqbal, M. T. and Quaicoe, J. E., "Hydrokinetic Energy Conversion Systems and Assessment of Horizontal and Vertical Axis Turbines for River and Tidal Applications: A Technology Status Review," Applied Energy 86, 1823-1835 (2009).

[2] Khan, M. J., Iqbal, M. T. and Quaicoe, J. E., "River Current Energy Conversion Systems: Progress, Prospects and Challenges," Renewable and Sustainable Energy Reviews 12, 2177-2193 (2008).

[3] Scott, G., "Mapping and Assessment of the United States Ocean Wave Energy Resource," Electric Power Research Institute Final Report 1024637, (Dec. 2011).

[4] Previsic, M., "System Level Design, Performance, Cost and Economic Assessment - Alaska River In-Stream Power Plants," EPRI RP 006 Alaska Electric Power Research Institute, (Oct. 31, 2008).

[5] Spillman, Jr., W. B. "Sensing and Processing for Smart Structures," Proc. IEEE 84(1), 68–77 (1996).

[6] Watkins, S. E., Sanders, G. W., Akhavan, F. and Chandrashekhara, K., "Modal Analysis using Fiber Optic Sensors and Neural Networks for Prediction of Composite Beam Delamination," Smart Materials and Structures 11(4), 489-495 (2002).

[7] Okafor, A. C., Chandrashekhara K. and Jiang, Y. P., "Delamination Prediction in Composite Beams with Built-in Piezoelectric Devices using Modal Analysis and Neural Network," Smart Materials and Structures 5, 338-47 (1996).

[8] Watkins, S. E., Akhavan, F., Dua, R.. Chandrashekhara, K. and Wunsch, D. C., "Impact-Induced Damage Characterization of Composite Plates using Neural Networks," Smart Materials and Structures 16(2), 515-524 (2007).

[9] Zetterlind III, V. E., Watkins, S. E. and Spoltman, M. W., "Feasibility Study of Embedded Fiber-Optic Strain Sensing for Composite Propeller Blades," Proc. SPIE 4332, 143-152 (2001).

[10] Lunia, A., Isaac, K. M., Chandrashekhara, K. and Watkins, S. E., "Aerodynamic Testing of a Smart Composite Wing using Fiber Optic Sensing and Neural Networks," Smart Materials and Structures 9(6), 767-773 (2000).

[11] Robison, K. E., Watkins, S. E., Nicholas, J., Chandrashekhara, K. and Rovey, J. L., "Instrumented Composite Turbine Blade for Health Monitoring," Proc. SPIE 8347, (2012).

[12] Heckman, A. J., Rovey, J. L., Chandrashekhara, K., Watkins, S. E., Mishra, R. and Stutts, D., "Ultrasonic Underwater Transmission of Composite Turbine Blade Structural Health," Proc. SPIE 8343, (2012).

[13] Measures, R. M., "Advances Toward Fiber Optic based Smart Structures," Optical Engineering 32, 34-47 (1992).

[14] Zhao, W., Wang J., Wang A. and Claus R. O., "Geometric Analysis of Optical Fiber EFPI Sensor Performance," Smart Materials and Structures 7, 907-910 (1998).

[15] Davis, M. A., Kersey A. D., Sirkis J. and Friebele E. J., "Fiberoptic Bragg Grating Array for Shape and Vibration Mode Sensing," Smart Materials and Structures 5, 759-765 (1996).

[16] Dua, R. and Watkins, S. E., "Near Real-Time Analysis of Extrinsic Fabry-Perot Interferometric Sensors under Damped Vibration using Artificial Neural Networks," Proc. SPIE 7292, (2009).

[17] Ebel, W. and Mitchell, K., "Hardware Complexity for Extrinsic Fabry-Perot Interferometer Sensor Processing," Proc. SPIE 7650, (2010).

[18] Fonda, J. W., Watkins, S. E., Sarangapani, J. and Zawodniok, M., "Embeddable Sensor Mote for Structural Monitoring," Proc. SPIE 6932, (2008).

[19] Mitchell, K., Watkins, S. E., Fonda, J. W. and Sarangapani, J., "Embeddable Modular Hardware for Multi-Functional Sensor Networks," Smart Materials and Structures 16(5), N27-N34 (2007).

[20] Mitchell, K., Ebel, W. and Watkins, S. E., "Low-power Hardware Implementation of Artificial Neural Network Strain Detection for Extrinsic Fabry-Perot Interferometric Sensors under Sinusoidal Excitation," Optical Engineering 48(11), 114402 (2009).